Journal of Quantitative Spectroscopy & Radiative Transfer 227 (2019) 72–85

Contents lists available at ScienceDirect

Journal of Quantitative Spectroscopy & Radiative Transfer

journal homepage: www.elsevier.com/locate/jqsrt

On snowpack heating by solar radiation: A computational model

Leonid A. Dombrovsky[a,b,*], Alexander A. Kokhanovsky[c], Jaona H. Randrianalisoa[d]

[a] Joint Institute for High Temperatures, NCHMT, 17A Krasnokazarmennaya St, Moscow 111116, Russia
[b] University of Tyumen, 6 Volodarskogo St, Tyumen 625003, Russia
[c] VITROCISET Belgium SPRL, Bratustrasse 7, Darmstadt D-64293, Germany
[d] GRESPI Laboratory, The University of Reims, Champagne-Ardenne, 51687 Reims Cedex 2, France

ARTICLE INFO

Article history:
Received 15 January 2019
Revised 4 February 2019
Accepted 4 February 2019
Available online 5 February 2019

Keywords:
Solar radiation
Snow heating
Radiative transfer
Absorption and scattering
Computational model

ABSTRACT

A new approach to calculate the solar radiation transfer in absorbing and scattering snow and the resulting heating and possible partial melting of snow is suggested. The propagation of both the directional solar radiation and diffuse radiation from the sky is calculated using the transport approximation for the scattering phase function and two-flux method for radiative transfer of a diffuse component of the scattered radiation. A comparison with the direct Monte Carlo simulation of solar radiation transfer in a snowpack confirmed sufficiently good accuracy of the differential method. The calculated distribution of the absorbed radiation power is considered as a heat source in a transient energy equation to obtain the evolution of temperature profile in a snowpack during several solar days. The computational results obtained for the model problem as applied to heat transfer conditions typical of polar regions make clear a relative contribution of the visible and near-infrared spectral ranges and also the role of both radiative and convective cooling as well as continuous conductive heating of a deep snow layer. The effect of a sloping surface on solar heating of snow is also analyzed in the paper.

1. Introduction

Polar regions of our planet are undergoing rapid changes, including the decrease of ice/snow extent with corresponding impacts on polar environments [1,2]. The behavior of massive ice and snowpack under regular summer heating by solar radiation is one of the problems which is not well understood because of interaction of a variety of physical processes. The present paper is focussed on a particular problem of physical and computational modeling of snowpack heating by solar radiation.

There are many research papers concerning the spectral properties of snow, the snow albedo (including effects of atmospheric impurities), and the effects of heat transfer conditions on both microstructure and macroscopic properties of snow. However, only few publications are focused on modeling the combined radiative and conductive heat transfer in a snowpack. One should recall the interesting findings of the study by Brant and Warren [3] on a relatively deep penetration of shortwave solar radiation in a snowpack and night radiative cooling by emission of thermal infrared radiation to space occurring at the very top surface of the snow. The authors of [3] used the term “solid-state greenhouse” for this interesting phenomenon. Deep penetration of heat into the snowpack was discussed also by Liston and Winther [4]. In particular, they reported that about seven times more meltwater is produced subsurface compared to the surface for snow-covered areas in near coastal Antarctica. The most of studies including recent paper [5] employed some variants of the two-flux approximation (sometimes, without a separate consideration of collimated and diffuse components of the radiation field) and did not present the study of possible errors of this traditional approach. To the best of our knowledge, there is no complete computational model for both the spectral radiative transfer and alternating heating and cooling of a snowpack. We have not found an analysis of the role of the main physical parameters on computational results as well.

The main objective of the paper is twofold: (1) To develop an approximate but complete and reliable computational model for heating of snow by solar radiation and (2) To present the numerical results illustrating the influence of the main physical parameters on snow heating.

A choice of particular theoretical models seems to be natural for the beginning of a study concerning the interaction of spectral radiative transfer in absorbing and scattering snow and transient heat transfer in a snow layer. The simplest approaches are used to calculate wide range optical properties of snow, transfer of an oblique solar irradiation in snow, and evolution of temperature profile in a snow layer. However, the complete model takes into

* Corresponding author at: Joint Institute for High Temperatures, NCHMT, 17A Krasnokazarmennaya St, Moscow 111116, Russia.
E-mail address: ldombr@yandex.ru (L.A. Dombrovsky).

https://doi.org/10.1016/j.jqsrt.2019.02.004
0022-4073/

Nomenclature

a	radius of particle
C	normalized coefficients
c	specific heat capacity
d	thickness
E	function introduced by Eq. (12)
$\tilde{E}$	function introduced by Eq. (1e)
F	size distribution of ice grains
$f_{1,2}$	functions introduced by Eq. (1d)
f_v	volume fraction
G	irradiance
h	convective heat transfer coefficient
I	radiation intensity
J	diffuse radiation intensity
k	thermal conductivity
L	latent heat of melting
l	distance between particles
m	complex index of refraction
N	number of rays
n	index of refraction
P, p	radiative power
Q	efficiency factor
q	radiative flux
$R_{1,2}$	functions introduced by Eq. (1e)
T	temperature
t	time
x	diffraction parameter
y	coefficient in Eq. (1a)
z	normal coordinate

Greek symbols

α	absorption coefficient
β	extinction coefficient
δ	declination of the Sun
ε	coefficient in Eq. (23c)
ζ	integration variable in Eqs. (1a) and (1b)
$\tilde{\zeta}$	function introduced by Eq. (1e)
θ	zenith angle
ϑ	sloping angle
κ	index of absorption
λ	radiation wavelength
μ	cosine of an angle
$\bar{\mu}$	asymmetry factor of scattering
ν	coefficient in Eq. (2)
ρ	density
σ	scattering coefficient
τ	optical thickness
ξ	parameter introduced by Eq. (18a)
Φ	scattering phase function
$\phi_{1,2}$	functions introduced by Eq. (1c)
φ	local latitude
χ	hour angle
ψ	function introduced by Eq. (27b)
ω	scattering albedo

Subscripts and superscripts

0	initial
a	absorption
air	air
av	average
diff	diffuse
i	incident
m	melting
ni	near-infrared range
s	scattering
sky	sky
sl	sloping
sol	solar
t	total
th	thermal
tr	transport
vis	visible range
w	spectral window
λ	spectral

account both the direct solar radiation and diffuse radiation from the sky, the convective cooling of snow typical of polar regions and the middle-infrared radiative cooling, the local melting and solidification of snow, and also the effect of sloping of snow surface on time variation of the surface temperature.

Several alternative approaches are considered for the spectral optical properties of snow and radiative transfer calculations in an optically thick layer of snow. This makes possible a verification of analytical methods employed in the present study. It is proved that relatively simple methods chosen in this work are sufficiently accurate for the problem under consideration.

2. Spectral optical properties of snow

2.1. Optical constants of ice in the visible and near-infrared

Two spectral optical constants are usually considered as real and imaginary parts of the complex index of refraction, $m(\lambda)=n(\lambda)-i\kappa(\lambda)$, where n is the index of refraction, κ is the index of absorption, and λ is the wavelength [6]. Spectral behavior of the indices of refraction and absorption are not independent of each other but satisfy the Kramers-Krönig relation [7]. Particularly, the index of refraction is almost constant in the spectral ranges of a very low absorption as that for water ice in the visible range. The spectral optical constants of ice obtained by Warren and Brandt [8] are plotted in Fig. 1. The wavelength range shown in this figure is the most important one for the radiative heating problem under consideration.

The extremely low value of κ in the visible and a significant increase of absorption index in the near-infrared range determine the specific spectral properties of ice grains and snow. In particular, the high value of snow albedo is a result of almost perfect spectral transparency of pure ice [9–11]. Obviously, even very small amount of impurities such as atmospheric aerosol particles may increase significantly the value of κ, and this affects strongly the observed albedo of snow [12–14]. One can also recommend more recent papers on the specific problem of snow albedo [15–19]. In the present paper, the solar heating of pure snow is considered and the effects of impurities are beyond the scope of the paper.

2.2. Spectral optical properties of snow

Theoretical modeling of optical properties of various turbid media is often based on the classical Mie theory for spherical particles [20–22]. The size of snow particles is much greater that the wavelength of solar radiation, and the shape of these particles may be very complex. Therefore, the geometrical optics (GO) approximation and some other advanced methods are used to calculate optical properties of single particles and the resulting properties of snow [23–25]. Alternative approaches for optical properties of ice grains of complex shape can be found in papers [26–30]. However, for the sake of simplicity, one should not forget about physically sound analytical approximations suggested in early papers [31–37].

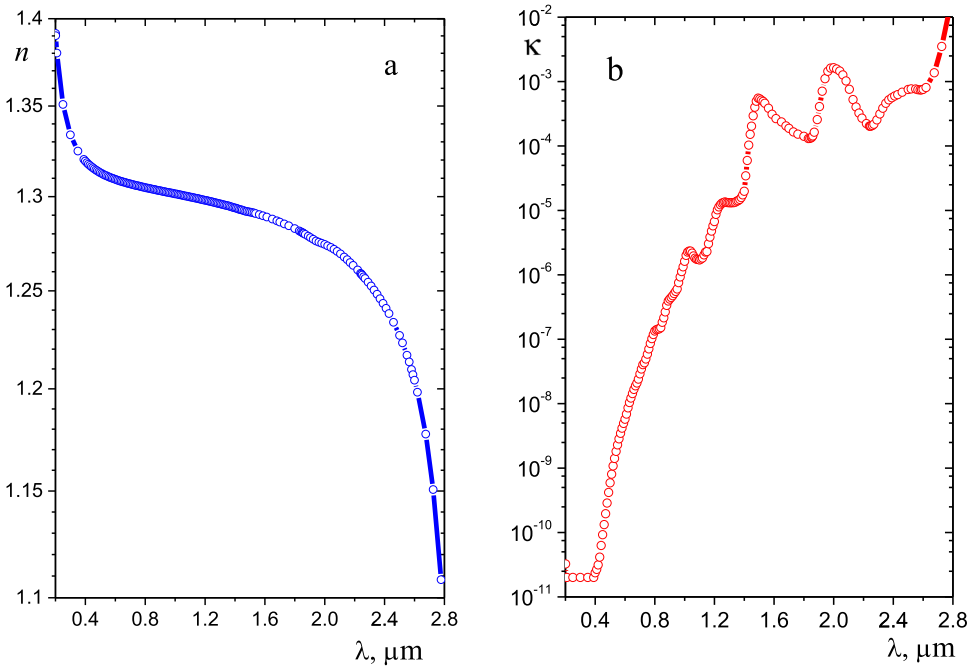

Fig. 1. Spectral optical constants of ice: a – index of refraction, b – index of absorption.

In the present paper, the spherical ice grains of different size are considered instead of ice particles of complex shape and orientation. The calculations are performed for ice grains of radius $a = 50$ μm, 100 μm, and 200 μm. These variants can be treated as those corresponding to different snow morphology. The case of nonspherical particles can be treated as well. However, we focus this study on snowpack heating and the problem of nonsphericity of ice grains is of a secondary importance for us. For the same reason we do not account for possible snow pollution. The study of corresponding effects will be a subject of our future work.

The most general solution for the optical properties of homogeneous spherical particles is given by the Mie theory. However, the ice grains considered are much greater in size that the wavelength. This makes reasonable to consider the GO approximation as the main tool in this work. At the same time, the Mie theory with the use of computer code published in [35] and described also in [37] is used for the reference calculations.

There is no need in analysis of all the properties of single ice grains because only limited number of the main parameters are used in a computational model suggested by us for the radiative transfer in snow. The simple approach based on the transport approximation for scattering phase function [35–38] is employed in radiative transfer calculation of the present paper. Therefore, only two dimensionless characteristics of absorption and scattering of single particles are calculated: the absorption efficiency factor, Q_a, and the so-called transport efficiency factor of scattering, $Q_s^{tr} = Q_s \cdot (1 - \bar{\mu})$, where $\bar{\mu}$ is the asymmetry factor of scattering. The values of transport efficiency factor of extinction, $Q_{tr} = Q_a + Q_s^{tr}$, and transport albedo of the particle, $\omega_{tr} = Q_s^{tr}/Q_{tr}$ are also considered. The above mentioned characteristics depend on spectral optical constants and also on the diffraction (size) parameter $x = 2\pi a/\lambda$ introduced in the Mie theory. The spectral dependence of optical constants makes reasonable to use dimensional values of radiation wavelength and particle radius in subsequent analysis.

The results of calculations using the GO solution obtained by Kokhanovsky and Zege [33] are compared with calculations based on the Mie theory in Fig. 2. The values of Q_a and ω_{tr} are chosen for this comparison. Fig. 2 indicates that GO can be used to calculate both the absorption efficiency factor and transport albedo of single scattering for ice grains of various size. As a result, the important value of transport extinction coefficient, $Q_{tr} = Q_a/(1 - \omega_{tr})$, can be also obtained using the GO solution for the case of $\kappa << n$ [33]:

$$Q_a = 2 - Q_s \quad Q_s = 1 + \tilde{Q}_s \quad \bar{\mu} = (1 + y)/\left(1 + \tilde{Q}_s\right) \tag{1a}$$

$$\tilde{Q}_s = \frac{1}{2}\sum_{j=1}^{2}\int_0^{\pi/2} f_j(\zeta)\sin 2\zeta\, d\zeta \quad y = \frac{1}{2}\sum_{j=1}^{2}\int_0^{\pi/2}\frac{\phi_j(\zeta)\sin 2\zeta\, d\zeta}{1 - 2R_j\tilde{E} + R_j^2\tilde{E}^2} \tag{1b}$$

where

$$\phi_j(\zeta) = \tilde{E}\left(1 - R_j\right)^2\cos 2\left(\zeta - \tilde{\zeta}\right) + R_j\left(1 - \tilde{E}^2\right)\cos 2\zeta + 2R_j^2\left(\tilde{E} - \cos 2\tilde{\zeta}\right)\tilde{E}\cos 2\zeta \tag{1c}$$

$$f_j(\zeta) = R_j + \tilde{E}\left(1 - R_j\right)^2/\left(1 - R_j\tilde{E}\right) \tag{1d}$$

$$R_1 = \frac{\tan^2\left(\zeta - \tilde{\zeta}\right)}{\tan^2\left(\zeta + \tilde{\zeta}\right)} \quad R_2 = \frac{\sin^2\left(\zeta - \tilde{\zeta}\right)}{\sin^2\left(\zeta + \tilde{\zeta}\right)}$$
$$\tilde{E} = \exp\left(-4\kappa x\sqrt{1 - \tilde{\zeta}^2}\right) \quad \tilde{\zeta} = \frac{\cos\zeta}{n} \tag{1e}$$

To avoid numerical errors of direct calculations by Eqs. (1a)–(1e) at $Q_a < 10^{-5}$, one can use the following approximation which is correct in the case of $\kappa x << 1$:

$$Q_a = 4\nu\kappa x \quad \nu = \frac{2}{3}\left[n^3 - \left(n^2 - 1\right)^{3/2}\right] \tag{2}$$

One can also use the following expression recommended in [37,39] for arbitrary values of x:

$$Q_a = \frac{4n}{(n+1)^2}\left[1 - \exp\left(-4\kappa x\right)\right] \tag{3}$$

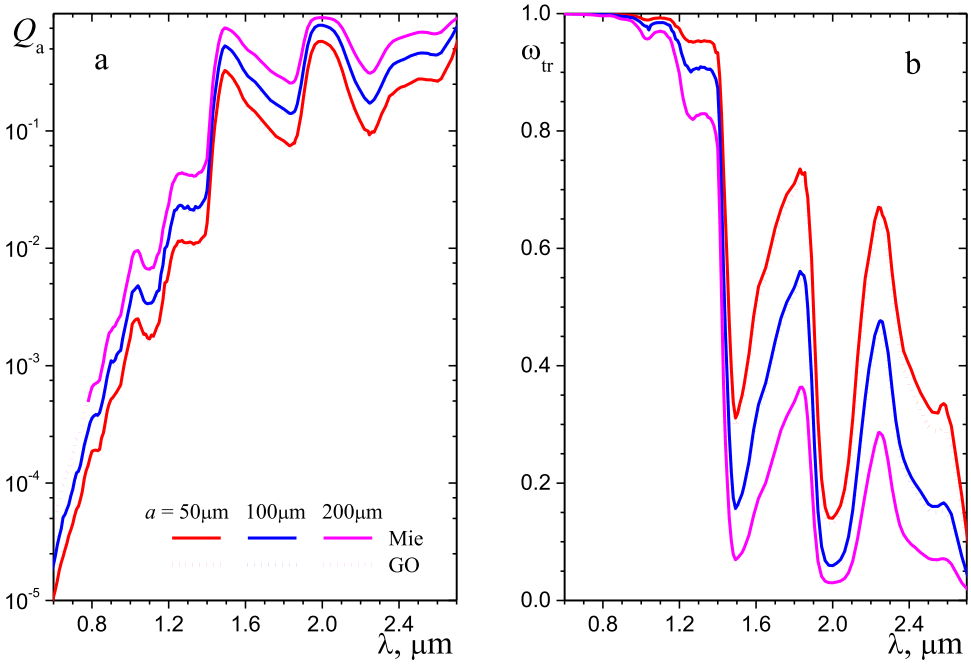

Fig. 2. Optical properties of single ice grains: a – efficiency factor of absorption, b – transport albedo.

Note that Eq. (3) is sufficiently accurate for droplets and solid particles of different chemical compositions in the spectral range of semitransparency of the particle substance [39–42]. Eqs. (2) and (3) give practically the same values of Q_a for ice grains under consideration.

One can see in Fig. 2b that light scattering highly predominates very weak absorption in the visible spectral range. This results in a strong reflection of visible solar radiation from the snow surface and relatively small contribution of this spectral range to the heating of snow surface layer. At the same time, the remaining (not reflected) visible part of the collimated solar radiation forms almost diffuse radiation field in the snow which can be described on the basis of simple differential models. It should be noted that the visible light is absorbed relatively far from the snow surface, and a contribution of this effect to heating deep layers of snow may be considerable. On the contrary, the reflection of near-infrared solar radiation from the snow surface is smaller as compared to that in the visible. Also there is a strong contribution of this spectral range to the radiation power absorbed in the surface layer of snow. The role of multiple scattering is important in the near-infrared range as well, and the transformation of the direct solar radiation into the diffuse one because of multiple scattering takes place at small distances from the snow surface. The strong multiple scattering of radiation in snow makes it possible to use simple approximations for the scattering phase function (like the mentioned transport approximation), which leads to significant simplifications in radiative transfer calculations.

The ice grains are large in comparison with the radiation wavelength. Also it is assumed that the hypothesis of independent scattering is true [43–46]. It means that each particle absorbs and scatters the radiation in exactly the same manner as if other particles do not exist. In addition, there is no systematic phase relation between partial waves scattered by individual particles during the observation time interval, so that the intensities of the partial waves can be added without regard to phase. In other words, each particle is in the far-field zones of all other particles, and scattering by individual particles is incoherent.

In the case of polydisperse spherical ice grains, the following equations are true [37]:

$$\left\{\alpha_\lambda, \sigma_\lambda^{\mathrm{tr}}, \beta_\lambda^{\mathrm{tr}}\right\} = 0.75 f_{\mathrm{v}} \int_{a_{\min}}^{a_{\max}} \left\{Q_{\mathrm{a}}, Q_{\mathrm{s}}^{\mathrm{tr}}, Q_{\mathrm{tr}}\right\} a^2 F(a)\mathrm{d}a \Big/ \int_{a_{\min}}^{a_{\max}} a^3 F(a)da \quad f_v = \rho_{snow}/\rho_{ice} \tag{4a}$$

where α_λ, $\sigma_\lambda^{\mathrm{tr}}$, and $\beta_\lambda^{\mathrm{tr}} = \alpha_\lambda + \sigma_\lambda^{\mathrm{tr}}$ are the spectral absorption coefficient, the transport scattering coefficient, and the transport extinction coefficient, f_{v} is the volume fraction of effective ice grains in snow, ρ_{snow} and ρ_{ice} are the densities of snow and bulk ice, respectively, $F(a)$ is the size distribution of ice grains. In many cases, one of the mean radii $a_{\mathrm{j,j-1}}$ can be used to reduce the problem to the monodisperse approach [37]:

$$\left\{\alpha_\lambda, \sigma_\lambda^{\mathrm{tr}}, \beta_\lambda^{\mathrm{tr}}\right\} = 0.75 f_v \left\{Q_a, Q_s^{\mathrm{tr}}, Q_{\mathrm{tr}}\right\} / a_{j,j-1}$$

$$a_{j,j-1} = \int_{a_{\min}}^{a_{\max}} a^j F(a)da \Big/ \int_{a_{\min}}^{a_{\max}} a^{j-1} F(a)da \quad j = 1, 2, 3 \tag{4b}$$

In the case of $j = 3$, we have the Sauter mean radius a_{32}, but it is known that this choice is not the universal one. Moreover, the monodisperse approximation with any $a_{\mathrm{j,j-1}}$ may be inapplicable even in not too complex problems [37,47].

The following size distribution was used in subsequent estimates:

$$F(a) \sim 1 - (a - a_{\min})^2 / a_{\mathrm{av}}^2 \quad a_{\mathrm{av}} = (a_{\min} + a_{\max})/2 \tag{5}$$

The calculations for wide size distribution with $a_{\min} = 50$μm and $a_{\max} = 150$μm showed that the value of $a_{21} = 105$μm is good as an equivalent radius of monodisperse ice grains. This is demonstrated in Fig. 3, where the coefficients normalized per unit volume fraction, $C_{\mathrm{a}} = \alpha_\lambda / f_{\mathrm{v}}$ and $C_{\mathrm{s}}^{\mathrm{tr}} = \sigma_\lambda^{\mathrm{tr}} / f_{\mathrm{v}}$, are presented. It should be noted that the choice of a_{21} is determined by scattering only because Q_{a} is almost directly proportional to the grain size and the value of C_{a} is weakly sensitive to the grain size. Note that transport albedo of monodisperse snow, $\omega_\lambda^{\mathrm{tr}}$, is the same as that of single scattering. It was shown in [37] that the value of an equivalent radius of monodisperse particles in independent of the one-modal size distribution.

Obviously, similar results can be obtained for various size distributions and the calculations of spectral properties of polydisperse ice grains can be replaced by appropriate calculations for monodisperse grains. This possibility is used in the present paper.

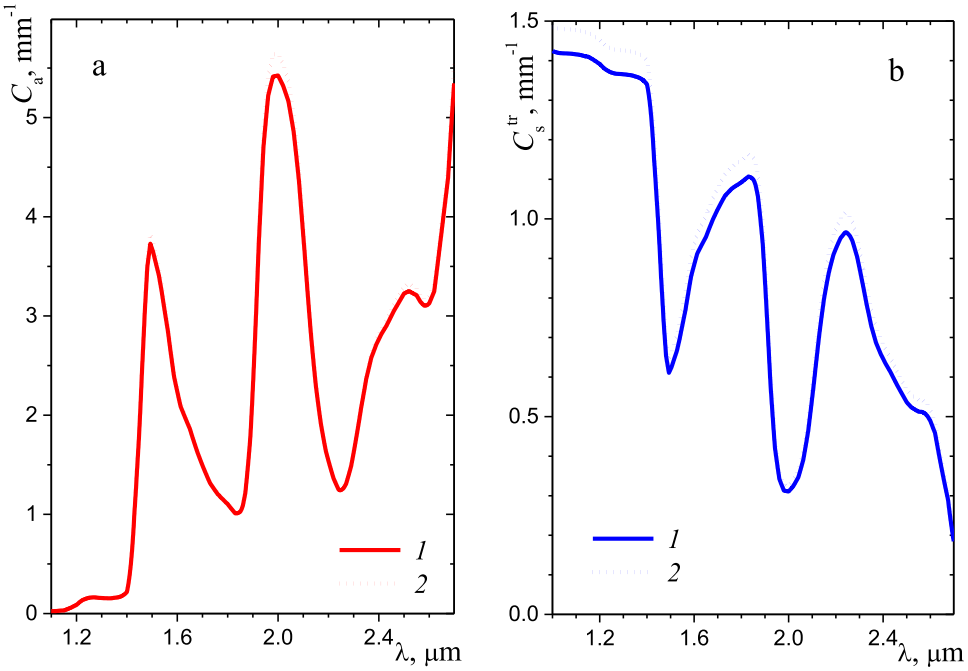

Fig. 3. Optical properties of polydisperse ice grains: 1 – complete calculation, 2 – monodisperse approximation with $a = a_{21}$.

3. Solution to the radiative transfer problem in snowpack

The computational models which can be employed in calculations of the electromagnetic radiation propagation in a snowpack can be classified into two categories, i.e., models based on radiative transfer theory (see, e.g., [48,49]) and models based on direct ray-tracing techniques [50–52]. A discussion of these approaches including the model based on two coupled volume-averaged radiative transfer equations [53–57] as applied to radiative transfer in snowpack can be found in [58].

The traditional radiative transfer equation (RTE) or relatively simple differential models are definitely more appropriate to obtain the profile of absorbed radiation power, $P(z)$, in a snow layer. Obviously, the general problem is a spectral one, and the following general relations are true:

$$P(z) = \int_{\lambda_{\min}}^{\lambda_{\max}} p(z,\lambda)\mathrm{d}\lambda \qquad p(z,\lambda) = \alpha_\lambda(z) G_\lambda(z) \tag{6}$$

where G_λ is the spectral irradiance, $\lambda_{\min}$ and $\lambda_{\max}$ are the boundaries of the wavelength range that makes the greatest contribution to the solar heating of snow.

The radiative transfer problem for an optically thick layer of a semi-transparent snow is characterized by multiple scattering. In this case, the details of angular distribution of spectral radiation intensity in single scattering are not important and one can use the so-called transport approximation, which appears to be highly successful method to solve many applied problems of neutron transport and radiative transfer [36–38,59,60]. According to this approximation, the scattering phase function in the RTE is replaced by a sum of the isotropic component and the term describing the peak of forward scattering:

$$\Phi_\lambda(\mu_0) = (1-\bar{\mu}_\lambda) + 2\bar{\mu}_\lambda \delta(1-\mu_0) \tag{7}$$

where μ_0 is the cosine of scattering angle, $\bar{\mu}_\lambda$ is the anisotropy factor of scattering of a medium, and $\delta(1-\mu_0)$ is the Dirac delta-function. With the use of transport approximation, the RTE can be written in the same way as that for isotropic scattering, i.e., with $\Phi_\lambda \equiv 1$ but with the "transport" scattering and extinction coefficients defined as follows:

$$\sigma_\lambda^{\mathrm{tr}} = \sigma_\lambda(1-\bar{\mu}_\lambda) \qquad \beta_\lambda^{\mathrm{tr}} = \alpha_\lambda + \sigma_\lambda^{\mathrm{tr}} = \beta_\lambda - \sigma_\lambda\bar{\mu}_\lambda \tag{8}$$

where σ_λ and β_λ are the ordinary coefficients of scattering and extinction.

In the case of oblique solar irradiation, the radiation field in a snow layer is three-dimensional. Obviously, for the distribution of the absorbed power over the thickness of the snow layer, only the solar zenith angle is important and it does not matter which side of the normal the Sun is located. Let us imagine that the radiative flux is uniformly distributed over the surface of a cone with the same zenith angle at the vertex. Of course, in this case the power profile of the absorbed radiation will be the same. In other words, the original problem is equivalent to the 1-D axisymmetric problem of the oblique irradiation along the cone surface. The described technique has already been recently used in a study on attenuation of solar radiation by water mists and sprays [61]. The axial symmetry enables one to integrate the original transport RTE over the azimuth angle. The resulting equation and boundary conditions for a snow layer can be written as follows (see, e.g., [37,62,63]):

$$\mu\frac{\partial I_\lambda}{\partial z} + \beta_\lambda^{\mathrm{tr}} I_\lambda = \frac{\sigma_\lambda^{\mathrm{tr}}}{2}\int_{-1}^{1} I_\lambda(z,\mu)\mathrm{d}\mu \quad \mu = \cos\theta \quad 0 < z < d \tag{9a}$$

$$I_\lambda(0,\mu) = I_\lambda^{\mathrm{sol}}(\mu_{\mathrm{i}})\delta(\mu_{\mathrm{i}}-\mu) + I_\lambda^{\mathrm{sky}} \quad I_\lambda(d,-\mu) = 0 \quad \mu,\mu_{\mathrm{i}} > 0 \tag{9b}$$

where I_λ is the spectral radiation intensity, $\mu_{\mathrm{i}} = \cos\theta_{\mathrm{i}}$ is the direction of incident solar light, I_λ^{sol} is the collimated solar radiation intensity transmitted through the atmosphere, I_λ^{sky} is the diffuse radiation from the sky. In contrast to recent paper [64] on radiative heating of relatively thin layers of ice and snow, the volumetric self-emission of thermal radiation in a thick snowpack is neglected in Eq. (9a). It should be also noted that Eq. (9a) is written for the particular case of an isotropic medium when the coefficients of this equation do not depend on direction. The current time, t, is not a variable of the radiative transfer problem, the value of t is just a parameter of this particular problem. Note that the above

mentioned spectral irradiance is defined as follows:

$$G_\lambda(z,\mu_\mathrm{i}) = \int_{-1}^{1} I_\lambda(z,\mu)\mathrm{d}\mu \tag{10}$$

To simplify further transformations, consider the case of an optically uniform snow layer when both the absorption coefficient and transport scattering coefficient do not depend on coordinate z. The linearity of the RTE makes possible a separate consideration of additive contribution from the direct solar radiation and radiation from the sky. Consider first the transfer of direct solar radiation. Obviously, Eqs. (9a) and (9b) can be written in the dimensionless form:

$$\mu\frac{\partial \bar{I}_\lambda}{\partial \tau_\lambda^{\mathrm{tr}}} + \bar{I}_\lambda = \frac{\omega_\lambda^{\mathrm{tr}}}{2}\bar{G}_\lambda \quad \bar{G}_\lambda\left(\tau_\lambda^{\mathrm{tr}}\right) = \int_{-1}^{1} \bar{I}_\lambda\left(\tau_\lambda^{\mathrm{tr}},\mu\right)\mathrm{d}\mu \tag{11a}$$

$$\bar{I}_\lambda(0,\mu) = \delta(\mu_\mathrm{i}-\mu) \quad \bar{I}_\lambda(\infty,-\mu) = 0 \quad \mu,\mu_\mathrm{i} > 0 \tag{11b}$$

There are two simplifications in Eqs. (11a,b): the boundary condition at $z=d$ is replaced by the same condition at $\tau_\lambda^{\mathrm{tr}} \to \infty$ (this can be done for optically thick snowpacks), the dimensionless values of radiation intensity, $\bar{I}_\lambda = I_\lambda / I_\lambda^{\mathrm{sol}}(\mu_\mathrm{i})$, current optical thickness, $\tau_\lambda^{\mathrm{tr}} = \int_0^z \beta_\lambda^{\mathrm{tr}}(z)\mathrm{d}z$, and transport albedo, $\omega_\lambda^{\mathrm{tr}}(z) = \sigma_\lambda^{\mathrm{tr}}(z)/\beta_\lambda^{\mathrm{tr}}(z)$, are introduced.

Following the usual technique [65], the radiation intensity is represented as a sum of the diffuse component $\bar{J}_\lambda$ and the term corresponding to the directional solar radiation:

$$\bar{I}_\lambda\left(\tau_\lambda^{\mathrm{tr}},\mu\right) = \bar{J}_\lambda\left(\tau_\lambda^{\mathrm{tr}},\mu\right) + E_\lambda^{\mathrm{i}}\delta(\mu-\mu_\mathrm{i}) \quad E_\lambda^{\mathrm{i}} = \exp\left(-\tau_\lambda^{\mathrm{tr}}/\mu_\mathrm{i}\right) \tag{12}$$

The spectral irradiance can be also written as a sum of two components:

$$\bar{G}_\lambda\left(\tau_\lambda^{\mathrm{tr}},\mu_\mathrm{i}\right) = \bar{G}_\lambda^{\mathrm{diff}}\left(\tau_\lambda^{\mathrm{tr}},\mu_\mathrm{i}\right) + E_\lambda^{\mathrm{i}} \quad \bar{G}_\lambda^{\mathrm{diff}} = \int_{-1}^{1}\bar{J}_\lambda\mathrm{d}\mu \tag{13}$$

A similar approach to the problem of oblique incidence of solar radiation was considered in [61,66].

The mathematical problem statement for the diffuse component of radiation intensity is as follows:

$$\mu\frac{\partial \bar{J}_\lambda}{\partial \tau_\lambda^{\mathrm{tr}}} + \bar{J}_\lambda = \frac{\omega_\lambda^{\mathrm{tr}}}{2}\left(\bar{G}_\lambda^{\mathrm{diff}} + E_\lambda^{\mathrm{i}}\right) \tag{14a}$$

$$\bar{J}_\lambda(0,\mu) = \bar{J}_\lambda(\infty,-\mu) = 0 \quad \mu > 0 \tag{14b}$$

The source term on the right of Eq. (14a) does not depend on angular variable. According to [67], it enables further simplification of the problem with the use of two-flux approximation.

For the diffuse radiation from the sky, one should use another normalization, $\bar{I}_\lambda = I_\lambda / q_\lambda^{\mathrm{sky}}$, and replace the term $\delta(\mu_\mathrm{i}-\mu)$ by 1 in Eq. (11b). As a result, the following equations are true:

$$\mu\frac{\partial \bar{J}_\lambda}{\partial \tau_\lambda^{\mathrm{tr}}} + \bar{J}_\lambda = \frac{\omega_\lambda^{\mathrm{tr}}}{2}\bar{G}_\lambda^{\mathrm{diff}} \tag{15a}$$

$$\bar{J}_\lambda(0,\mu) = 1 \quad \bar{J}_\lambda(\infty,-\mu) = 0 \quad \mu > 0 \tag{15b}$$

The spectral component of the absorbed radiation power given by Eq. (6) can be written as:

$$p(z,\lambda) = \alpha_\lambda(z)\left[\bar{G}_\lambda^{\mathrm{i}}(z)q_{\lambda,\mathrm{i}}^{\mathrm{sol}} + \bar{G}_\lambda^{\mathrm{sky}}(z)q_\lambda^{\mathrm{sky}}\right] \tag{16}$$

The superscripts “i” and “sky” are introduced here to distinguish the dimensionless irradiance functions for the solar and sky radiation.

3.1. Approximate analytical solution for absorbed radiation power

One of the differential approximations can be employed to calculate the diffuse component of the radiation field [38]. These approximations are based on simple assumptions concerning the angular dependence of the spectral radiation intensity. As a result, one can deal with a limited number of functions $\bar{J}_\lambda^{\mathrm{i}}(\tau_\lambda^{\mathrm{tr}})$ instead of function $\bar{J}_\lambda(\tau_\lambda^{\mathrm{tr}},\mu)$ and turn to the system of the ordinary differential equations by the use of integration of RTE. The analysis of the simplest differential approximations [37] and direct comparison with the exact numerical solution for physically similar problem [68] showed that the two-flux (Schwarzschild-Schuster) method is preferable as compared with P_1 approximation (Eddington method). This is explained by a discontinuous angular dependence of radiation intensity at the irradiated boundary of the medium.

The following representation of $\bar{J}_\lambda(\tau_\lambda^{\mathrm{tr}},\mu)$ is considered in the two-flux method:

$$\bar{J}_\lambda\left(\tau_\lambda^{\mathrm{tr}},\mu\right) = \begin{cases}\bar{J}_\lambda^{-}\left(\tau_\lambda^{\mathrm{tr}}\right), & -1<\mu<0\\ \bar{J}_\lambda^{+}\left(\tau_\lambda^{\mathrm{tr}}\right), & 0<\mu<1\end{cases} \tag{17}$$

Integrating Eq. (14a) separately over the intervals $-1 < \mu < 0$ and $0 < \mu < 1$, one can obtain the following boundary-value problem for the diffuse irradiance $\bar{G}_\lambda^{\mathrm{i,diff}}(\tau_\lambda^{\mathrm{tr}}) = \bar{J}_\lambda^{-}(\tau_\lambda^{\mathrm{tr}}) + \bar{J}_\lambda^{+}(\tau_\lambda^{\mathrm{tr}})$:

$$-\left(\bar{G}_\lambda^{\mathrm{i,diff}}\right)'' + \xi_\lambda^2\bar{G}_\lambda^{\mathrm{i,diff}} = 4\omega_\lambda^{\mathrm{tr}}E_\lambda^{\mathrm{i}} \quad \xi_\lambda = 2\sqrt{1-\omega_\lambda^{\mathrm{tr}}} \tag{18a}$$

$$\left(\bar{G}_\lambda^{\mathrm{i,diff}}\right)'(0) = 2\bar{G}_\lambda^{\mathrm{i,diff}}(0) \quad \left(\bar{G}_\lambda^{\mathrm{i,diff}}\right)'(\infty) = 0 \tag{18b}$$

The above equations are true at arbitrary variations of ξ_λ and $\omega_\lambda^{\mathrm{tr}}$ with the current optical thickness $\tau_\lambda^{\mathrm{tr}}$, and the problem (18a,b) can be easily solved numerically. However, it is interesting to obtain an analytical solution of the problem in the case of uniform optical properties of snow. The analytical solution to the boundary-value problem (18a,b) at $\xi_\lambda \neq 1/\mu_\mathrm{i}$ can be written as follows [66]:

$$\bar{G}_\lambda^{\mathrm{i,diff}}\left(\tau_\lambda^{\mathrm{tr}},\mu_\mathrm{i}\right) = \frac{4\omega_\lambda^{\mathrm{tr}}}{\xi_\lambda^2 - 1/\mu_\mathrm{i}^2}\left(E_\lambda^{\mathrm{i}} - \frac{2+1/\mu_\mathrm{i}}{2+\xi_\lambda}E_\lambda^{\mathrm{diff}}\right)E_\lambda^{\mathrm{diff}} = \exp\left(-\xi_\lambda\tau_\lambda^{tr}\right) \tag{19}$$

where μ_i should be considered as a parameter. There are two different exponential functions in Eq. (19). The first one, E_λ^{i}, is related with a contribution of the collimated solar radiation, whereas the second one, $E_\lambda^{\mathrm{diff}}$, appears in the term corresponding to the diffuse component of the radiation field.

For the diffuse radiation from the sky, the following simple expression can be easily obtained [36]:

$$\bar{G}_\lambda^{\mathrm{sky}}\left(\tau_\lambda^{\mathrm{tr}}\right) = 2E_\lambda^{\mathrm{diff}} \tag{20}$$

A comparison of functions $E_\lambda^{\mathrm{i}}(\tau_\lambda^{\mathrm{tr}})$ and $E_\lambda^{\mathrm{diff}}(\tau_\lambda^{\mathrm{tr}})$ indicates that propagation depth of collimated radiation (defined as a distance from the snow surface at which the irradiance decreases e times) is less than the propagation depth of diffuse radiation component when $\omega_\lambda^{\mathrm{tr}} > 0.75$. This condition is satisfied in the wavelength range of $\lambda < 1.4\mu\mathrm{m}$.

3.2. Some computational results and verification of the analytical solution

It is convenient to consider a model problem to understand the main special features of the obtained solution for radiative transfer in a snowpack. Obviously, a contribution of the direct solar radiation to the snowpack heating is predominant as compared with the sky radiation. Therefore, it is sufficient to consider the absorbed

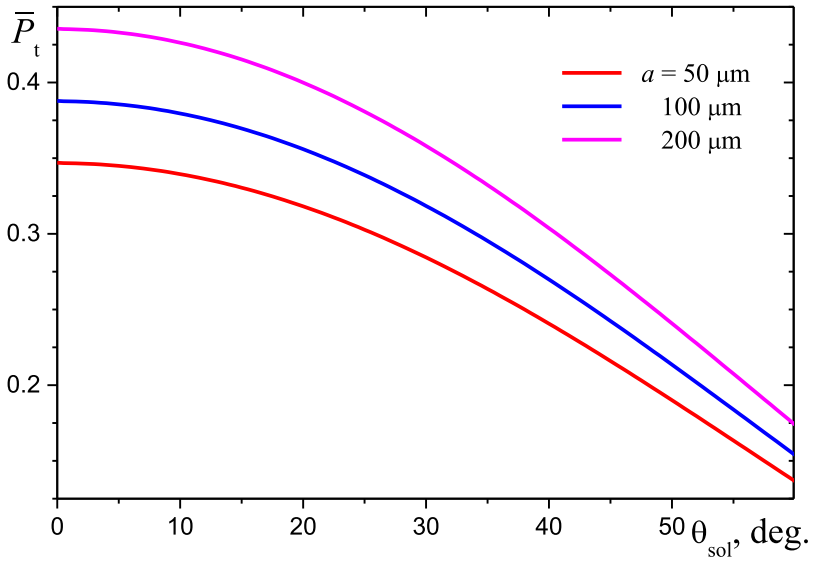

Fig. 4. The normalized radiative power absorbed in optically thick snowpack.

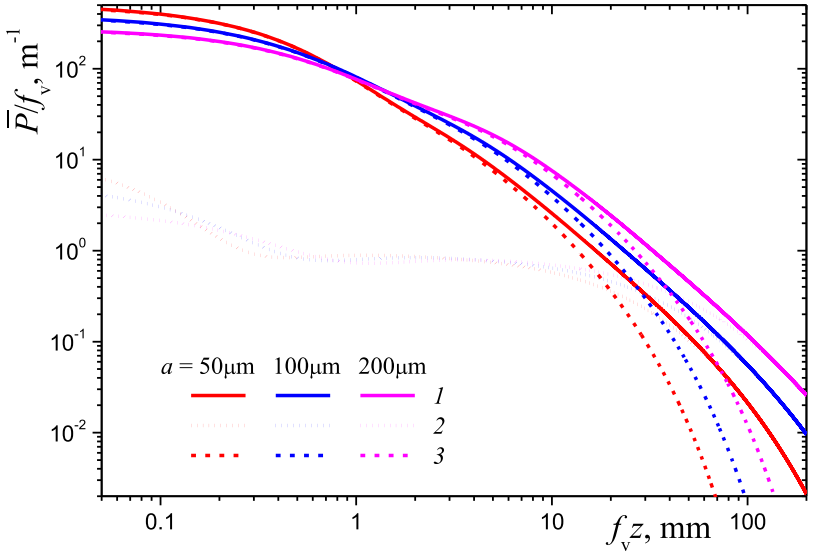

Fig. 5. The profiles of normalized absorbed radiation power in snowpack: *1* – the integral value ($\bar{P}$), *2* – the visible range contribution ($\bar{P}_{vis}$), *3* – the near-infrared contribution ($\bar{P}_{ni}$).

power of solar radiation at various values of zenith angle θ_{sol}. It is assumed in the model problem that the spectrum of the incident solar radiation is similar to the blackbody radiation at temperature $T_{sol} = 6000$K. The calculated relative values of the integral (over the spectrum) radiation power, $\bar{P}_t = \int_0^\infty P(z)dz / \int_{\lambda_{min}}^{\lambda_{max}} I_b(T_{sol}, \lambda)d\lambda$ (I_b is the Planck function), absorbed in a snowpack containing ice grains of different size are presented in Fig. 4. It is known that the spectrum of solar radiation is quite different from the model one at large zenith angles. Therefore, this range of θ_{sol} is not shown in Fig. 4. As one can expect, the main part of solar radiation is reflected from the snowpack because of almost total reflection of the visible radiation. One can see that the value of $\bar{P}_t$ decreases considerably with the zenith angle, whereas the effect of ice grain size is insignificant.

The depth of the radiation propagation into the snowpack can be illustrated by calculations at normal incidence (see Fig. 5). The contributions of the visible range ($\lambda < 0.78$μm) and the near-infrared range to the absorbed radiation power are calculated separately:

$$\bar{P}(z) = \bar{P}_{vis}(z) + \bar{P}_{ni}(z) \quad \left\{\bar{P}_{vis}, \bar{P}_{ni}\right\} = \left\{P_{vis}, P_{ni}\right\} \Big/ \int_{\lambda_{min}}^{\lambda_{max}} I_b(T_{sol}, \lambda)d\lambda \tag{21}$$

The universal coordinates $f_v z$ and $\bar{P}/f_v$ are used in Fig. 5 to present simultaneously the results for various values of f_v (the ratio of snow density to ice density). At realistic value of $f_v = 0.33$, the near-infrared radiation is absorbed mainly in a thin surface layer of snowpack, whereas the visible radiation is absorbed almost uniformly in the layer of thickness about 60 mm and its contribution to heating deep layers of snowpack is expected to be considerable. The depth of the radiation penetration increases with the grain size, but this effect is not strong. Therefore, the subsequent calculations will be performed at $a = 100$ μm.

The main difficulty of the problem under consideration is to determine the full profile of absorbed radiation in a thick snowpack. This is much more complicated than the calculation of snow

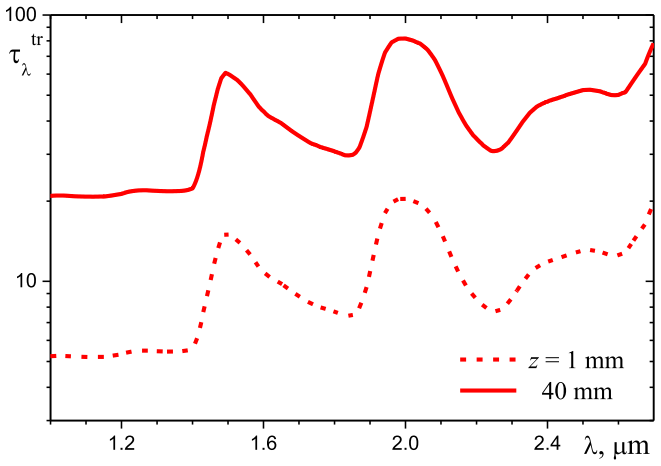

Fig. 6. Transport optical thickness of snow layers.

albedo or radiation absorption in a thin layer of snow considered in many papers. Of course, the desired profile of the absorbed power of radiation is easily obtained using the analytical solution obtained above. However, an estimate of the error associated with the employed approximate physical model of radiation transfer is not an easy task.

The most obvious, but not the main, mathematical difficulty becomes clear already when trying to numerically solve the problem (18a,b). To obtain reliable results, the optical thickness of the medium at the computational grid step should be much less than unity. At the same time, Fig. 6 shows that transport optical thickness of the snow layer at $f_v = 0.33$ is very large already at $z = 40$mm and the value of τ_λ^{tr} is about four times different at $\lambda = 1\mu$m and $\lambda = 2\mu$m. This difficulty can be overcome in the case of the two-flux method, but obtaining reliable numerical results using more accurate high-order method of discrete ordinates becomes almost impossible.

Therefore, the Monte Carlo simulation with a great number of rays is used as a reference solution in the present paper. Two characteristic wavelengths and three values of zenith angle were chosen for verification of the suggested approach using the direct numerical simulation of solar radiation transfer in a snowpack. The forward collision-based Monte Carlo method is employed. The details of this method can be found in textbooks [62,63], in review paper by Farmer and Howell [69], and recent papers [66,70–72]. In the forward Monte Carlo (MC) algorithm of simulation of ray propagation in an absorbing and scattering medium, a large number of stochastic incident rays N_i of wavelength λ and direction cosine μ_i with respect to the outward normal at the snowpack surface is followed throughout the medium until either they leave the medium at the same boundary or are absorbed within the medium. The spectral component of the absorbed radiation power is calculated as:

$$\bar{p}_\lambda(z) = N_{i,a}/(N_i \Delta z) \tag{22}$$

where $N_{i,a}$ is the number of absorbed rays within a computational cell of thickness Δz.

A comparison between MC calculations at $f_v = 0.33$ and those using the suggested approximate model presented in Fig. 7 indicates good qualitative agreement between the data obtained using these quite different methods.

One should recall that MC calculations are very time-consuming and it is not realistic to use more than 10^8 rays in the calculations. Most likely, it is insufficient in the case of $\lambda = 0.6\mu$m at $z > 100$mm because very high albedo of the medium and large optical depth of the light propagation. Therefore, a relatively strong decrease in the absorbed power at $z > 200$ mm is related with the computational limitations of the MC simulation. So, one can say about sufficiently good accuracy of the relatively simple method suggested in the present paper. The latter statement is additionally supported by an expected compensation of specific errors in spectral calculations by the integration of the absorbed radiation power over the wavelength.

4. Computational model for heating of snowpack by solar radiation

Generally speaking, there are various combined thermal or related processes in a snowpack and many of them should be involved in a complete transient computational model for snow heating. As an example, one should recall the processes of ice sublimation and diffusion of water vapor through a snow layer. These processes appear to be important for the snow microstructure, which determines macroscopic snow properties. The related

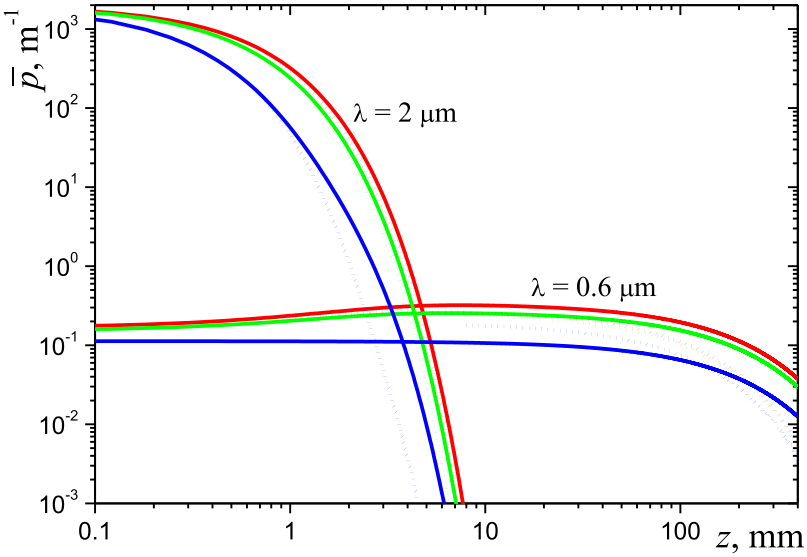

Fig. 7. The profiles of normalized absorbed radiation power in snowpack at typical wavelengths solid lines approximate solution, dotted lines – MC simulation; Upper curves – normal incidence, middle curves – $\theta_{sol} = 30°$, lower curves – $\theta_{sol} = 60°$.

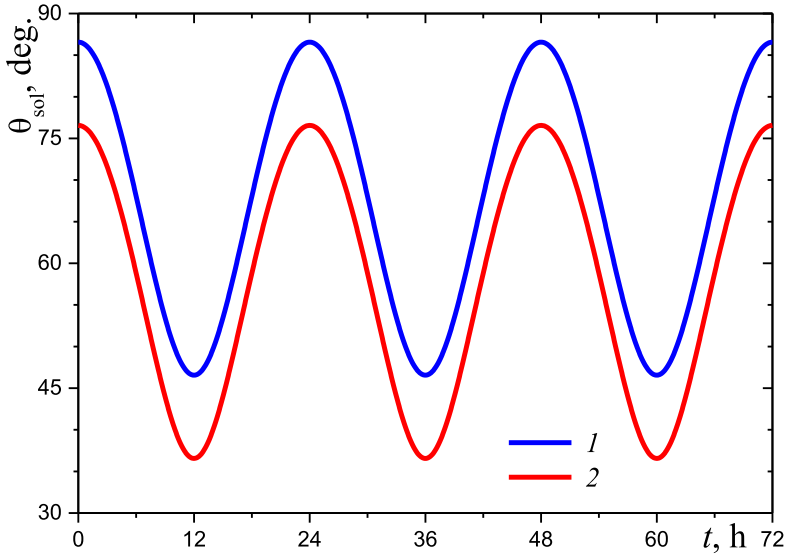

Fig. 8. Time variation of solar zenith angle considered in the case problem: *1* – horizontal surface, *2* – sloping surface at $\vartheta_{sl} = 10°$.

problems are analyzed in detail in [72,73]. Strictly speaking, a contribution of both sublimation and diffusion processes to the combined heat transfer in deep layers of snow should be also taken into account [58,74–76]. However, a study of these processes is beyond the scope of the present paper.

The simplest transient energy equation for temperature, $T(t, z)$, in the snow layer of thickness $d_{th} >> d$ and the accompanying initial and boundary conditions can be written as follows:

$$\rho c \frac{\partial T}{\partial t} = \frac{\partial}{\partial z}\left(k \frac{\partial T}{\partial z}\right) + P \qquad t > 0 \quad 0 < z < d_{th} \tag{23a}$$

$$T(0, z) = T_0(z) \tag{23b}$$

$$z = 0, \; -k \frac{\partial T}{\partial z} = h(T_{air} - T) - \varepsilon\pi \int_{\lambda_{w1}}^{\lambda_{w2}} I_b(T, \lambda) d\lambda \quad z = d_{th}, \; \frac{\partial T}{\partial z} = 0 \tag{23c}$$

where z is the coordinate measured from the open surface of a snowpack, ρ, c, and k are the density, the specific (per unit mass) heat capacity, and the thermal conductivity of snow, $T_{air}(t)$ is the temperature of air above the snow layer, $h(t)$ is the convective heat transfer coefficient. The condition of thermal insulation at the boundary $z = d_{th}$ means that we neglect heat transfer by conduction at $z > d_{th}$. Of course, the value of d_{th} increases with time and it should be estimated using additional calculations. The time dependence of heat transfer coefficient is determined by a variation of wind speed.

The last term in the right-hand side of the boundary condition at $z = 0$ is the mid-infrared radiative cooling due to thermal radiation of snowpack surface in the atmospheric window of $\lambda_{w1} < \lambda < \lambda_{w2}$ ($\lambda_{w1} = 8$ μm, $\lambda_{w2} = 13$ μm) [77–79]. The radiative cooling is limited during the night time when it is not compensated by solar mid-infrared radiation. Therefore, the coefficient ε varies from zero in the day time to the unity at night. The absorbed radiation power, $P(z)$, at arbitrary conditions of solar irradiation of snow is calculated using the approximate analytical solution obtained is Section 3 of the paper.

When solving the model problem, the calculations can be carried out at constant or variable values of ρ, c, and k from the literature. The latent heat of ice melting, $L = 0.34$MJ/kg, is taken into account using an equivalent additional heat capacity, Δc, in narrow temperature range of $T_m - \Delta T < T < T_m + \Delta T$ (where $T_m = 273$K is the ice melting temperature, $\Delta T << T_m - T_0$) as it was done in [80–83] for physically similar melting and solidification problems. The following simple variant of this approach is employed in the present study:

$$\Delta c = \frac{L}{\Delta T}(1 - |T_m - T|/\Delta T) \tag{24}$$

The heat transfer calculations should be interrupted at $T = T_m + \Delta T$. A correct choice of ΔT value is determined by the interval of the computational grid and the time step of numerical solution to problem (23a)–(23c).

Obviously, it is difficult to choose a realistic initial profile of temperature, $T_0(z)$, for the heat transfer calculations. Fortunately, the effect of this temperature profile decreases with time. It will be shown below, that the choice of $T_0(z)$ makes no difference for the snow temperature after about four hours from the conventional initial time moment.

An implicit finite-difference scheme of the second order of spatial approximation was used in the calculations. The specific combination of a strong decrease of heat generation rate with the distance from the snow surface and rather deep propagation of heat in the snow layer due to long-time conduction makes it necessary to use a detailed and strongly non-uniform computational grid and double precision calculations. The results obtained were verified using variations of the computational parameters of the numerical procedure.

5. Numerical results

It is interesting to analyze the computational results obtained at realistic parameters of a snowpack solar heating. Some results of such calculations are presented below. The wide range of snow density variation from $\rho = 100$kg/m^3 to 550 kg/m^3 leads to the corresponding variations in thermal properties of snow. Obviously, the volumetric heat capacity, ρc, is directly proportional to the density, whereas the thermal conductivity of snow exhibits more strong increase with the snow density. In addition, at the same snow density, variations in snow microstructure can change thermal conductivity by a factor of two. Thermal conductivity of snow

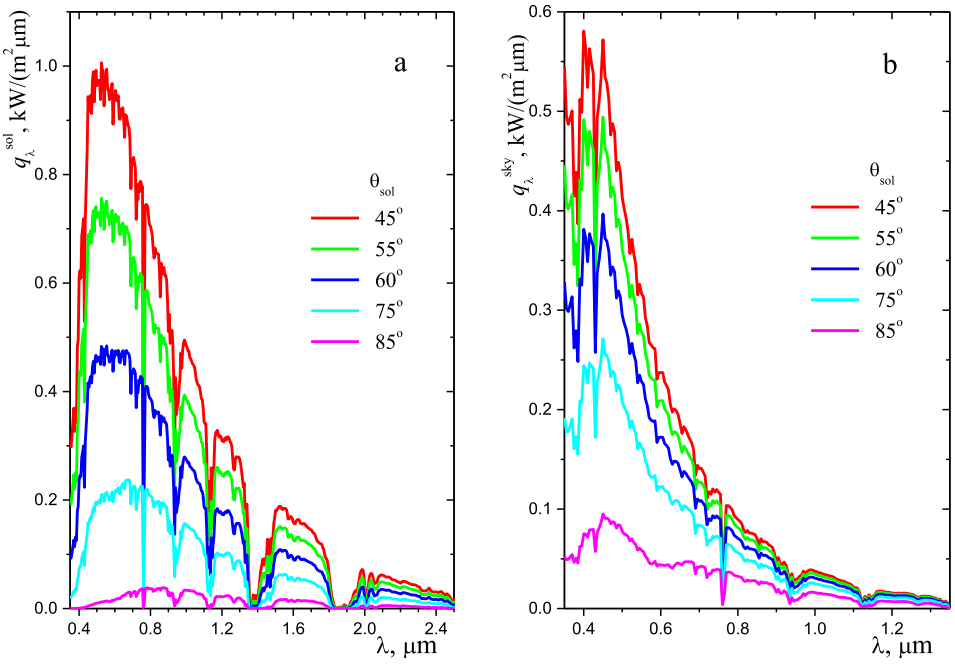

Fig. 9. The spectral radiative flux at the earth surface a – direct radiation from the Sun, b – diffuse radiation from the clear sky.

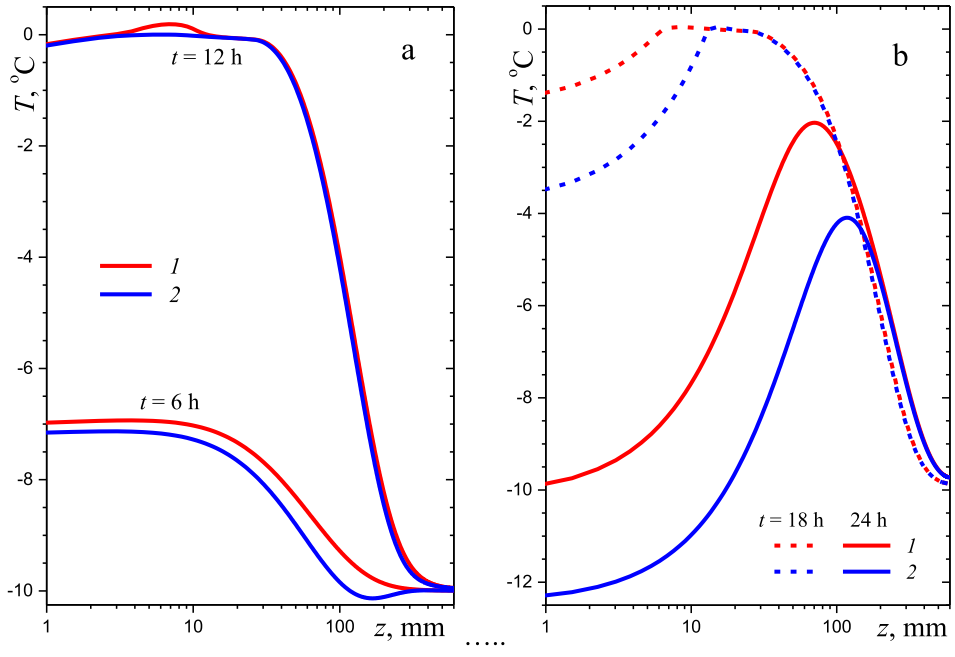

Fig. 10. Typical profiles of temperature in snowpack (a) before the noon and (b) after the noon: *1* – h_{max} = 10W/(m^2 K), *2* – 15 W/(m^2 K).

has been studied in many papers [74,84–93]. The most of the results obtained are discussed in recent review paper [94]. It was shown that thermal conductivity is almost directly proportional to the square of density and varies from $k = 0.04$W/(m K) to 1 W/(m K). The temperature variations of thermal properties of snow are relatively small and the effect of temperature on snow density and thermal properties is not considered in the case problem. The following constant values of $k = 0.2$W/(m K) and $\rho c = 0.6$MJ/(m^{3}K) corresponding to the volume fraction of ice grains of $f_v = 0.33$ were used in subsequent calculations.

In the midsummer (summer solstice), the current declination of the Sun is equal to $\delta = 23.44^o$. This value of δ is used to calculate the solar zenith angle:

$$\cos\theta_{sol} = \sin\varphi\sin\delta + \cos\varphi\cos\delta\cos\chi \tag{25}$$

where φ is the local latitude and χ is the hour angle. The value of $\varphi = 70^o$ is considered in subsequent calculations. The following relation is used to determine the value of χ for the current time, t, measured in hours from the midnight:

$$\chi = \pi|1 - t_1/12| \qquad t_1 = t - 24\lfloor t/24\rfloor \tag{26}$$

where symbol $\lfloor\rfloor$ denotes the floor function. The resulting variation of θ_{sol} with the local solar time is shown in Fig. 7. The effect of a

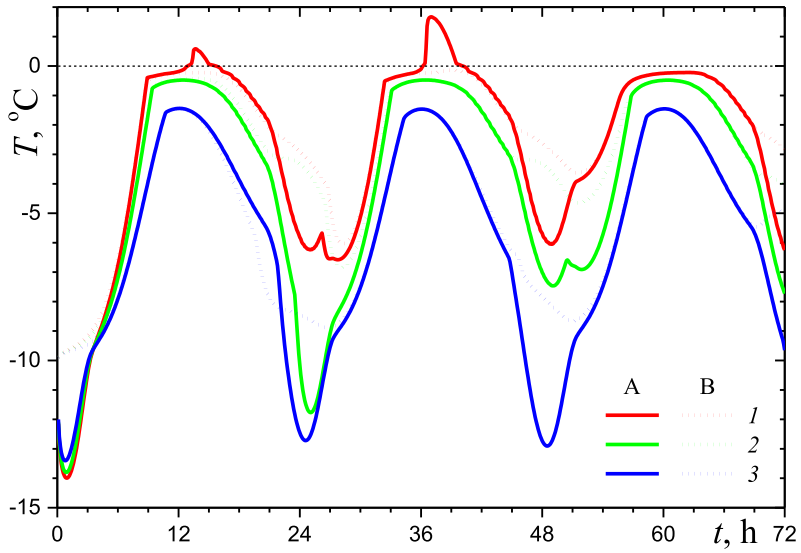

Fig. 11. The effect of wind on time variation of snowpack surface temperature: *1* – h_{max} = 8 W/(m^2 K) (very weak wind), *2* – 10W/(m^2 K) (weak wind), *3* – 15W/(m^2 K) (moderate wind); A – complete calculation, B without radiative cooling.

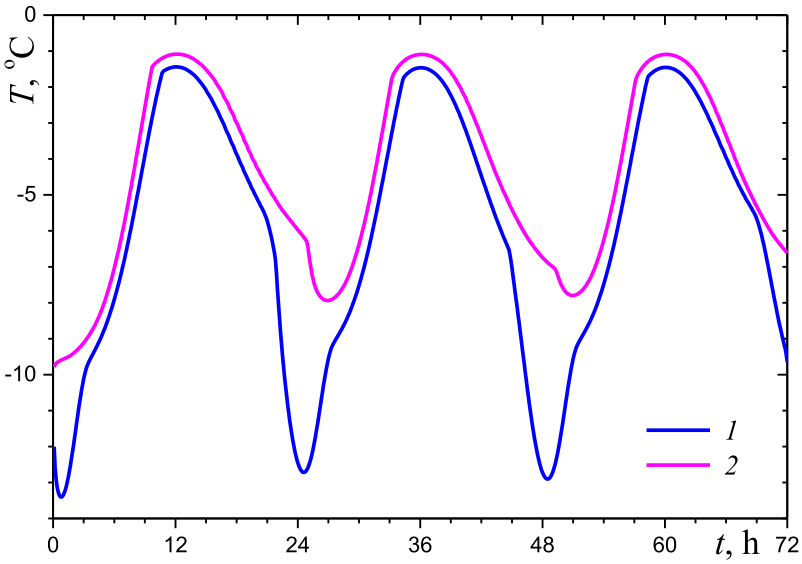

Fig. 12. Effect of sloping of snowpack surface on the time variation of surface temperature *1* – horizontal surface, *2* – sloping surface ($\vartheta_{sl} = 10°$). Calculations at h_0 = 15W/(m^2 K).

sloping surface of snow is also considered below. There are many possible orientations of the sloping surface with respect to visible path of the Sun. The simplest orientation can be treated as a variation of the declination angle. Time variation of the solar zenith angle for such irradiated surface with a sloping angle $\vartheta_{sl} = 10^o$ is also shown in Fig. 8.

The spectral radiative flux from the Sun and clear sky to the horizontal earth surface are presented in Fig. 9. The spectral dependences were calculated using the SBDART code [95]. The choice of solar zenith angles is determined by the case problem parameters. Generally speaking, a contribution of direct solar radiation is much greater than that of diffuse radiation from the sky. However, it is not the case for visible light at solar zenith angles $\theta_{sol} > 60^o$. Therefore, the sky radiation is taken into account in the calculations.

The following analytical expressions for the everyday variation of coefficients of convective heat transfer and radiative cooling are used in the calculations:

$$h = h_{min} + (h_{max} - h_{min})\psi(\theta_{sol}) \quad \varepsilon = 1 - F(\theta_{sol}) \tag{27a}$$

$$\psi(\theta_{sol}) = \begin{cases} 1, & 0 \le \theta_{sol} < 4\pi/9 \\ 0.5 - 0.5\sin(18\theta_{sol} - 8.5\pi), & 4\pi/9 \le \theta_{sol} < \pi/2 \end{cases} \tag{27b}$$

It is assumed in Eq. (27) that the midnight conditions approach gradually starting from $\theta_{sol} = 80^o$. Note that the values of heat transfer coefficient of h_{max} = 10W/(m^2 K) and 15 W/(m^2 K) correspond approximately to a weak wind (with a speed less that about 1–2 m/s) and to a moderate wind of speed about 3 m/s, respectively [96,97], whereas h_{min} = 6 W/(m^2 K) can be used for the windless weather.

The temperature profiles in snowpack calculated for the first day at $T_0 = T_{air}(z) = -10$ °C are presented in Fig. 10. One can see

that snowpack is heated rather fast in the morning and reaches the melting temperature at noon. A further evolution of the snowpack temperature depends strongly on wind speed. In the afternoon, the maximum temperature of snow is predicted at the distance about 15 mm from the snow surface at 6 pm and $h_{\max} = 15$ W/(m^2 K). The evening and night cooling of snowpack takes place for the surface layer of thickness from 15 mm to about 120 mm (for the windy weather), whereas a continuous heat conduction leads to further heating of deep layers of the snowpack.

The computational results for the three-day variation of snow surface temperature are presented in Fig. 11. One can see almost periodic variation of the temperature with a great difference between the day and the night. The effects of both the convective heat transfer in windy weather and the radiative cooling of a snowpack surface are significant and cannot be ignored. It is interesting that radiative cooling is partially compensated by a relatively long convective heating. The latter may lead to the unexpectedly strong surface heating and even melting as compared with the computational predictions ignoring the radiative cooling. This physical result of combined transient heat transfer in a snowpack is obtained for the first time. Note that the details of temperature behavior near the melting temperature are explained by the finite value of $\Delta T = 0.1$K used in the model calculations.

Similar calculations for the better irradiated sloping surface of snowpack with $\vartheta_{\rm sl} = 10^\circ$ can be easily calculated by multiplying the directional radiative flux at solar zenith angle $\theta_{\rm sol}(t)$ by the ratio of $\cos(\theta^{\rm sl}_{\rm sol})/\cos(\theta_{\rm sol})$, where $\theta^{\rm sl}_{\rm sol}(t)$ is plotted in red in Fig. 8. According to Eq. (32), the conventional night-time conditions including the radiative cooling don't take place for the sloping surface considered. The overall effect of snow surface sloping on time variation of snowpack surface temperature is shown in Fig. 12. Obviously, the snow surface turned to the Sun exhibits a higher surface temperature of snowpack, especially in the time of large zenith angle of the Sun. It means that specific conditions of solar irradiation cannot be ignored even at sloping angle of $\vartheta_{\rm sl} = 10^{\rm o}$.

It is important that the above calculations for the case problem demonstrated the main possibilities of the computational model, which is expected to be a convenient and useful tool in further studies of snowpack solar heating.

6. Conclusions

The spectral optical properties of ice grains in a snowpack are analyzed using both the Mie theory and geometrical optics approximation. It was shown that geometrical optics is sufficiently accurate to obtain the optical properties of snow with assumed spherical ice grains in the visible and near-infrared spectral ranges.

A modified differential computational model for transfer of solar radiation in absorbing and scattering snow was suggested. The transport approximation for the scattering phase function and two-flux method for radiative transfer of a diffuse component of the scattered radiation formed a basis of this relatively simple model. A comparison with the direct Monte Carlo simulation of solar radiation transfer in a snowpack confirmed sufficiently good accuracy of the differential model.

The obtained profiles of the absorbed radiation power at different conditions of solar irradiation were used at the second stage of the problem solution to calculate the heat source in a transient energy equation. The numerical solution to the energy equation accompanied by the initial and boundary conditions enabled us to obtain the evolution of temperature profile in a snow layer during several solar days as applied to summer conditions in a polar region.

The computational results obtained for the case study makes clear a contribution of the visible and near-infrared solar radiation as well as the role of convective cooling or heating of snow, mid-infrared radiative cooling of snow surface, and continuous heating of deep snow layers due to heat conduction. The numerical results for the effect of a sloping snow surface on solar heating of snow were also obtained using the developed physical model and computational procedure. The numerical analysis indicates a deep heating of snowpack and relatively strong effect of wind and radiative cooling on surface temperature of snow. The calculations for the case problem demonstrated the main possibilities of the computational model, which is expected to be a convenient and useful tool in further studies of snowpack solar heating.

Conflict of interests

None declared.

Acknowledgments

The first author is grateful to the Russian Foundation for Basic Research (Grant No. 19-08-00238a) and the Russian Ministry of Education and Science (project no. 3.8191.2017/БЧ) for the financial support of the present study. The work of the second author has been supported by the European Space Agency in the framework of ESRIN contract No. 4000118926/16/I-NB Scientific Exploitation of Operational Missions (SEOM) Sentinel-3 Snow (Sentinel-3 for Science, Land Study 1: Snow). The authors acknowledge the ROMEO HPC Center at the University of Reims Champagne-Ardenne for providing HPC resources for the reference calculations. The authors are grateful to M. Lamare for providing data shown in Fig. 9.

References

[1] Barry R.G. and Hall-McKim E.A., Polar environments and global change, Cambridge Univ. Press, Cambridge, UK, 2018.
[2] Massom R, Lubiu D. Polar remote Sensing, Vol. II: ice sheets. Chichester, UK: Praxis; 2006.
[3] Brant RE, Warren SG. Solar-heating rates and temperature profiles in Antarctic snow and ice. J Glaciol 1993;39(131):99–110.
[4] Liston GE, Winther J-G. Antarctic surface and subsurface snow and ice melt fluxes. J Climate 2005;18(10):1469–81.
[5] Munneke PK, van den Broeke MR, Reijmer CH, Helsen MM, Boot W, Schneebeli M, Steffen K. The role of radiation penetration in the energy budget of the snowpack at Summit, Greenland. Cryosphere 2009;3(2):155–65.
[6] Born M, Wolf E. Principles of optics. 7th (expanded) ed. New York: Cambridge Univ. Press; 1999.
[7] Lucarini V, Saarinene JJ, Peiponen K-E, Vartainen EM. Kramers–Krönig relations in optical material Research, springer series in optical sciences. Berlin: Springer; 2005.
[8] Warren SG, Brandt RE. Optical constants of ice from the ultraviolet to the microwave: a revised compilation. J Geophys Res 2008;113(D14):D14220.
[9] Wiscombe WJ, Warren SG. A model for the spectral albedo of snow, I: pure snow. J Atmos Sci 1980;37:2712–33.
[10] Warren SG. Optical properties of snow, Rev. Geophys Space Phys 1982;20(1):67–89.
[11] Kokhanovsky AA, Zege EP. Scattering optics of snow. Appl Opt 2004;43(7):1589–602.
[12] Warren SG, Wiscombe WJ. A model for the spectral albedo of snow, II: snow containing atmospheric aerosols. J Atmos Sci 1980;37:2734–45.
[13] Chýlek P, Ramaswamy V, Srivastava V. Albedo of soot-containing snow. J Geophys Res – Oceans 1983;88(C15):10837–43.
[14] Warren SG, Clarke AD. Soot in the atmosphere and snow surface of Antarctica. J Geophys Res 1990;95(D2):1811–16.
[15] Aoki T, Aoki T, Fukabori M, Hachikibo A, Tashibana Y, Nishio F. Effects of snow physical parameters on spectral albedo and bidirectional reflectance of snow surface. J Geophys Res 2000;105(D8):10219–36.
[16] Gardner AS, Sharp MJ. A review of snow and ice albedo and the development of a new physically based broadband albedo parameterization. J Geophys Res–Earth Surf 2010;115(F1):F01009.
[17] Brandt RE, Warren SG, Clarke AD. A controlled snow-making experiment testing the relation between black carbon content and reduction of snow albedo. J Geophys Res–Atmos 2011;116(D8):D08109.
[18] Wang X, Pu W, Ren Y, Zhang X, Zhang X, Shi J, Jin H, Dai M, Chen Q. Observations and model simulations of snow albedo reduction in seasonal snow due to insoluble light-absorbing particles during 2014 Chinese survey. Atmos Chem Phys 2017;17:2279–96.
[19] Kokhanovsky A, Lamare M, Di Mauro B, Picard G, Arnaud L, Dumont M, Tuzet F, Brockmann C, Box JE. On the reflectance spectroscopy of snow. Cryosphere 2018;12(7):2371–82.

[20] van de Hulst HC. Light scattering by small particles. New York: Dover; 1981.
[21] Bohren CF, Huffman DR. Absorption and scattering of light by small particles. New York: Wiley; 1983.
[22] Hergert W, Wriedt T. The Mie theory: basics and applications. Berlin: Springer; 2012.
[23] Bi L, Yang P, Kattawar GW, Hu Y, Baum BA. Scattering and absorption of light by ice particles: solution by a new physical-geometrical optics hybrid method. J Quant Spectrsc Radiat Transfer 2011;112(9):1492–508.
[24] Borovoi A, Konoshonkin A, Kustova N. The physical-optics approximation and its application to light backscattering by hexagonal ice crystals. J Quant Spectrsc Radiat Transfer 2014;146:181–9.
[25] Lindqvist H, Martikainen J, Räbinä J, Penttilä A, Muinonen K. Ray optics for absorbing particles with application to ice crystals at near-infrared wavelengths. J Quant Spectrsc Radiat Transfer 2018;217:329–37.
[26] Grenfell T, Warren S. Representation of a nonspherical ice particle by a collection of independent spheres for scattering and absorption of radiation. J Geophys Res 1999;104(D24):31697–709.
[27] Neshyba SP, Grenfell TC, Warren SG. Representation of a nonspherical ice particle by a collection of independent spheres for scattering and absorption of radiation: 2. Hexagonal columns and plates. J Geophys Res 2003;108(D15):4448.
[28] Libois Q, Picard G, France JL, Arnaud L, Dumont M, Carmagnola CM, King MD. Influence of grain shape on light penetration in snow. Cryosphere 2013;7(6):1803–18.
[29] Räisänen P, Kokhanovsky A, Guyot G, Jourdan O, Nousiainen T. Parametrization of single-scattering properties of snow. Cryosphere 2015;9(3):1277–301.
[30] Ishimoto H, Adachi S, Yamaguchi S, Tanikawa T, Aoki T, Masuda K. Snow particles extracted from X-ray computed microtomography imagery and their single-scattering properties. J Quant Spectrsc Radiat Transfer 2018;209:113–28.
[31] Irvine WM. The asymmetry of the scattering diagram of a spherical particle. Commun Observ Leiden 1963;17(3):176–84.
[32] Irvine WM. Light scattering by spherical particles: radiation pressure, asymmetry factor, and extinction cross section. J Opt Soc Am 1964;55(1):16–21.
[33] Kokhanovsky AA, Zege EP. Local optical parameters of spherical polydispersions: simple approximations. Appl Opt 1995;34(24):5513–19.
[34] Kokhanovsky AA, Zege EP. Optical properties of aerosol particles: a review of approximate analytical solutions. J Aerosol Sci 1996;28(1):1–21.
[35] Dombrovsky LA. Radiation heat transfer in disperse systems. New York: Begell House; 1996.
[36] Dombrovsky LA, Baillis D. Thermal radiation in disperse Systems: an engineering approach. New York: Begell House; 2010.
[37] Dombrovsky LA. Approximate methods for calculating radiation heat transfer in dispersed systems. Therm Eng 1996;43(3):235–43.
[38] Dombrovsky LA. The use of transport approximation and diffusion-based models in radiative transfer calculations. Comput Therm Sci 2012;4(4):297–315.
[39] Dombrovsky LA. Spectral model of absorption and scattering of thermal radiation by droplets of diesel fuel. High Temp 2002;40(2):242–8.
[40] Dombrovsky LA, Lipiński W. Transient temperature and thermal stress profiles in semi-transparent particles under high-flux irradiation. Int J Heat Mass Transfer 2007;50(11–12):2117–23.
[41] Dombrovsky LA, Dembele S, Wen JX. A simplified model for the shielding of fire thermal radiation by water mists. Int J Heat Mass Transfer 2016;96:199–209.
[42] Dombrovsky LA, Dembele S, Wen JX. An infrared scattering by evaporating droplets at the initial stage of a pool fire suppression by water sprays. Infrared Phys Technol 2018;91:55–62.
[43] Kokhanovsky AA. Optics of light scattering media: problems and solutions. 3rd ed. Chichester (UK): Praxis; 2004.
[44] Mishchenko MI, Travis LD, Lacis AA. Multiple scattering of light by particles: radiative transfer and coherent backscattering. New York: Cambridge Univ. Press; 2006.
[45] Mishchenko MI. Electromagnetic scattering by particles and particle groups: an introduction. Cambridge (UK: Cambridge Univ. Press; 2014.
[46] Mishchenko MI. “Independent” and “dependent” scattering by particles in a multi-particle group. OSA Continuum 2018;1(1):243–60.
[47] Dombrovsky LA. Radiation of isothermal polydisperse layer. High Temp 1976;14(4):733–7.
[48] Leroux C, Lenoble J, Brogniez G, Hovenier JW, de Haan JF. A model for the bidirectional polarized reflectance of snow. J Quant Spectrsc Radiat Transfer 1999;61(3):273–85.
[49] Mishchenko M, Dlugach JM, Yanovitskiy EG, Zakharova NT. Bidirectional reflectance of flat, optically thick particulate layers: an efficient radiative transfer solution and applications to snow and soil surfaces. J Quant Spectr Radiat Transfer 1999;63(2–6):409–32.
[50] Kaempfer TU, Hopkins MA, Perovich DK. A three-dimensional microstructure-based photon-tracking model of radiative transfer in snow. J Geophys Res 2007;112(D24):D24113.
[51] Picard G, Arnaud L, Domine F, Fily M. Determining snow specific surface area from near-infrared reflectance measurements: numerical study of the influence of grain shape. Cold Regions Sci Technol 2009;56(1):10–17.
[52] Xiong C, Shi J, Ji D, Wang T, Xu Y, Zhao T. A new hybrid snow light scattering model based on geometrical optics theory and vector radiative transfer theory. IEEE Trans Geosci Remote Sensing 2015;53(9):4862–75.
[53] Gusarov AV. Homogenization of radiation transfer in two-phase media with irregular phase boundaries. Phys Rev B 2008;77(14):144201.
[54] Gusarov AV. A model of averaged radiation transfer in two-phase homogeneous medium. High Temp 2009;47(3):375–89.
[55] Gusarov AV. Model of radiative heat transfer in heterogeneous multiphase media. Phys Rev B 2010;81(6):064202.
[56] Lipiński W, Petrasch J, Haussener S. Application of spatial averaging theorem to radiative heat transfer in two-phase media. J Quant Spectrsc Radiat Transfer 2010;111(1):253–8.
[57] Lipiński W, Keene D, Haussener S, Petrasch J. Continuum radiative heat transfer modeling in media consisting of optically distinct components in the limit of geometrical optics. J Quant Spectrsc Radiat Transfer 2010;111(16):2474–80.
[58] Haussener S, Gergely M, Schneebeli M, Steinfeld A. Determination of the macroscopic optical properties of snow based on exact morphology and direct pore-level heat transfer modeling. J Geophys Res 2012;117(F3):F03009.
[59] Davison B. Neutron transport theory. London: Oxford University Press; 1957.
[60] Crosbie AL, Davidson GW. Dirac-delta function approximation to the scattering phase function. J Quant Spectrsc Radiat Transfer 1985;33(4):391–409.
[61] Dombrovsky LA, Solovjov VP, Webb BW. Attenuation of solar radiation by water mist and sprays from the ultraviolet to the infrared range. J Quant Spectrsc Radiat Transfer 2011;112(7):1182–90.
[62] Howell JR, Siegel R, Mengüç MP. Thermal radiation heat transfer. New York: CRC Press; 2010.
[63] Modest MF. Radiative heat Transfer. 3rd ed. New York: Acad. Press; 2013.
[64] Timofeev AM. Simulation of radiative heating of snow and ice coating. Thermophys Aeromech 2018;25(5):765–72.
[65] Sobolev VV. Light scattering in planetary atmospheres (International series of monographs in natural Philosophy, v. 76). New York: Pergamon Press; 1975.
[66] Dombrovsky LA, Randrianalisoa JH. Directional reflectance of optically dense planetary atmosphere illuminated by solar light: an approximate solution and its verification. J Quant Spectrsc Radiat Transfer 2018;208:78–85.
[67] Dombrovsky L, Randrianalisoa J, Baillis D. Modified two-flux approximation for identification of radiative properties of absorbing and scattering media from directional-hemispherical measurements. J Opt Soc Am A 2006;23(1):91–8.
[68] Dombrovsky LA, Randrianalisoa JH, Lipiński W, Baillis D. Approximate analytical solution to normal emittance of semi-transparent layer of an absorbing, scattering, and refracting medium. J Quant Spectrsc Radiat Transfer 2011;112(12):1987–99.
[69] Farmer JT, Howell JR. Comparison of Monte Carlo strategies for radiative transfer in participating media. Adv Heat Transfer 1998;31:333–429.
[70] Dombrovsky LA, Randrianalisoa JH, Lipiński W, Timchenko V. Simplified approaches to radiative transfer simulations in laser induced hyperthermia of superficial tumors. Comput Therm Sci 2013;5(6):521–30.
[71] Randrianalisoa JH, Dombrovsky LA, Lipiński W, Timchenko V. Effects of short-pulsed laser radiation on transient heating of superficial human tissues. Int J Heat Mass Transfer 2014;78:488–97.
[72] Pinzer BR, Schneebeli M, Kaempfer TU. Vapor flux and recrystallization during dry snow metamorphism under a steady temperature gradient as observed by time-lapse micro-tomography. Cryosphere 2012;6(5):1141–55.
[73] Kaempfer TU, Plapp M. Phase-field modelling of dry snow metamorphism. Phys Rev E 2009;79(2 Pt 1):031502.
[74] Riche F, Schneebeli M. Thermal conductivity of snow measured by three independent methods and anisotropy considerations. Cryosphere 2013;7(1):217–227.
[75] Ebner PP, Schneebeli M, Steinfeld A. Metamorphism during temperature gradient with undersaturated advective airflow in a snow sample. Cryosphere 2016;10(2):791–7.
[76] Ebner PP, Steen-Larsen HC, Stenni B, Schneebeli M, Steinfeld A. Experimental observation of transient $\delta^{18}O$ interaction between snow and advection airflow under various temperature gradient conditions. Cryosphere 2017;11(4):1733–43.
[77] Raman AP, Anoma MA, Zhu L, Rephaeli E, Fan S. Passive radiative cooling below ambient air temperature under direct sunlight. Nature 2014;515:540–4.
[78] Chen Z, Zhu L, Raman A, Fan S. Radiative cooling to deep sub-freezing temperatures through a 24-h day-night cycle. Nature Commun 2016;7:13729.
[79] Hossain MM, Gu M. Radiative cooling: principles, progress, and potentials. Adv Sci 2016;3:1500360.
[80] Dombrovsky LA, Dinh T-N. The effect of thermal radiation on the solidification dynamics of metal oxide melt droplets. Nucl Eng Des 2008;238(6):1421–9.
[81] Dombrovsky LA. Approximate model for break-up of solidifying melt particles due to thermal stresses in surface crust layer. Int J Heat Mass Transfer 2009;52(3–4):582–7.
[82] Dombrovsky LA, Nenarokomova NB, Tsiganov DI, Zeigarnik YuA. Modeling of repeating freezing of biological tissues and analysis of possible microwave monitoring of volumetric phase changes. Int J Heat Mass Transfer 2015;89:894–902.
[83] Dombrovsky LA. Steam explosion in nuclear reactors: droplets of molten steel vs core melt droplets. Int J Heat Mass Transfer 2017;107:432–8.
[84] Fukusako S. Thermophysical properties of ice, snow, and sea ice. Int J Thermophys 1990;11(2):353–72.
[85] Sturm M, Johnson J. Thermal conductivity measurements of depth hoar. J Geophys Res Solid Earth 1992;97(B2):2129–39.
[86] Sturm M, Holmgren J, König M, Morris K. The thermal conductivity of seasonal snow. J Glaciol 1997;43(143):26–41.
[87] Sturm M, Perovich DK, Holmgren J. Thermal conductivity and heat transfer through the snow on the ice of the Beaufort Sea. J Geophys Res 2002;107(C21):8043.

[88] Schneebeli M, Sokratov S. Tomography of temperature gradient metamorphism of snow and associated changes in heat conductivity. Hydrol Processes 2004;18(18):3655–65.
[89] Calonne N, Flin F, Morin S, Lesaffre B, du Roscoat SR, Geindreau C. Numerical and experimental investigations of the effective thermal conductivity of snow. Geophys Res Lett 2011;38(23):L23501.
[90] Shertzer RH, Adams EE. Anisotropic thermal conductivity model for dry snow. Cold Reg Sci Technol 2011;69(2–3):122–8.
[91] Löwe H, Riche F, Schneebeli M. A general treatment of snow microstructure exemplified by an improved relation for thermal conductivity. Cryosphere 2013;7(5):1473–80.
[92] Oldroyd HJ, Higgins CW, Huwald H, Selker JS, Parlange MB. Thermal diffusivity of seasonal snow determined from temperature profiles. Adv Water Resour 2013;55:121–30.
[93] Osokin NI, Sosnovskiy AV, Chernov RA. Effective thermal conductivity of snow and its variations. Earth's Cryosphere 2017;21(3):55–61.
[94] Arenson LU, Colgan W, Marshall HP. Physical, thermal, and mechanical properties of snow, ice, and permafrost. In: Snow and Ice-Related Hazards, Risk and Disasters; 2015. p. 35–75.
[95] Ricchiazzi P, Yang S, Gautier C, Sowle D. SBDART: a research and teaching software for plane-parallel radiative transfer in the earth atmosphere. Bull Am Meteorol Soc 1998;79(10):2101–14.
[96] Defraeye T, Blocken B, Carmeliet J. Convective heat transfer for exterior building surfaces: existing correlations and CFD modelling. Energy Convers Manage 2011;52(1):512–22.
[97] Mirsadeghi M, Cóstola D, Blocken B, Hensen JLM. Review of external convective heat transfer coefficient models in building energy simulation programs: implementation and uncertainty. Appl Therm Eng 2013;56(1–2):134–51.